Disorder and cluster formation during ion irradiation of Au nanoparticles in SiO_2

P. Kluth,[1,*] B. Johannessen,[1] G. J. Foran,[2] D. J. Cookson,[3] S. M. Kluth,[1] and M. C. Ridgway[1]
[1]*Department of Electronic Materials Engineering, Australian National University, Canberra ACT 0200, Australia*
[2]*Australian Nuclear Science and Technology Organization, Menai, Australia*
[3]*Australian Synchrotron Research Program, Building 434, 9700 South Cass Avenue, Argonne, Illinois 60439, USA*
(Received 23 February 2006; revised manuscript received 3 May 2006; published 11 July 2006)

Au nanoparticles (NPs) have been formed by ion beam synthesis in 600 nm thin SiO_2. Subsequently the NPs were irradiated with 2.3 MeV Sn ions at liquid nitrogen temperature. Samples were analyzed using extended x-ray absorption fine structure (EXAFS) spectroscopy and small angle x-ray scattering (SAXS) as a function of Sn irradiation dose. Transmission electron microscopy shows that the NPs largely retain their spherical shape upon irradiation. However, we observe a reduction in average NP size and a concomitant significant narrowing of the size distribution with increasing irradiation dose as consistent with inverse Ostwald ripening. At lower irradiation doses, significant structural disorder is apparent with an effective bond length expansion as consistent with amorphous material. At higher irradiation doses, EXAFS measurements indicate dissolution of a significant fraction of Au from the NPs into the SiO_2 matrix (as monomers) and the formation of small Au clusters (dimers, trimers, etc.). We estimate the volume fraction of such monomers/clusters. Ion irradiation thus yields disordering then dissolution of Au NPs.

DOI: 10.1103/PhysRevB.74.014202 PACS number(s): 61.46.Df, 61.10.Ht, 61.80.Jh, 61.10.Eq

I. INTRODUCTION

Nanoparticles (NPs) have received increasing attention over the last decade due to their interesting properties which can differ significantly from those of the corresponding bulk material. Such properties are generally related to the limited number of atoms within the NPs and the considerable surface to bulk ratio (SBR). This can lead to significant structural deviations as compared to "infinite" bulk material and a concomitant alteration of the NP physical properties.[1]

Ion implantation is a very versatile technique and has been widely used for NP fabrication (ion beam synthesis) as well as for structural modification of semiconductor based materials (ion irradiation). Whereas the influence of ion irradiation on the structure of bulk materials has been studied extensively and some understanding of the underlying mechanisms has been established,[2] only recently has the influence of ion irradiation on NPs been investigated and revealed a number of interesting phenomena. Simulations show that ion irradiation can significantly alter the evolution of the *size* distribution of NPs embedded in a matrix material, i.e., lead to narrowing due to inverse Ostwald ripening, and some experimental evidence has been reported for irradiated Au NPs using transmission electron microscopy[3,4] (TEM). At very high energies, where electronic stopping is dominant, a shape transformation from spherical to elongated rods has been observed for irradiated[5] Co NPs. The influence of ion irradiation on the *structure* of metallic NPs, however, has remained a widely unexplored area.

In this paper, the effect of ion irradiation on *size* and *structure* of Au NPs embedded in SiO_2 is investigated using a unique combination of extended x-ray absorption fine structure (EXAFS) spectroscopy and small angle x-ray scattering (SAXS). EXAFS provides a powerful tool for analysis of particles of nanometer dimensions giving accurate information about the average local atomic environment of the absorbing atom.[6] It is particularly sensitive to interatomic distances and local disorder and has been successfully utilized to resolve subtle NP structural details.[7] SAXS gives additional information about the NP size distribution and thus enables a size-dependent interpretation of the structural data obtained by EXAFS.

II. EXPERIMENTAL

First, we have grown 600 nm thick SiO_2 on Si (100) substrates using thermal oxidation in O_2. The amorphous SiO_2 layers were then sequentially implanted with ^{197}Au ions at 1.4 MeV to an ion dose of 5×10^{16} cm^{-2} and at 0.6 MeV to an ion dose of 2.5×10^{16} cm^{-2}. This yields a peak Au concentration of approximately 3 at. %. The implantations were performed at room temperature. Subsequently samples were annealed at 1000 °C for 1 h in a conventional quartz furnace to promote further precipitation and reduce irradiation-induced damage of the host material. A first set of samples (*series I*) was annealed in O_2 and a second set of samples (*series II*) was annealed in forming gas (95% N_2 and 5% H_2). It has previously been shown that the annealing atmosphere has a profound influence on the resulting NP size.[8] After formation the NPs were irradiated with ^{119}Sn ions at 2.3 MeV to ion doses between 1×10^{14} cm^{-2} and 1×10^{16} cm^{-2}. The energy was chosen such that essentially all Sn ions were stopped within the Si substrate, i.e., Sn-related impurity effects were negligible. The samples were maintained at liquid nitrogen temperature during ion irradiation. The Au concentration profiles were measured by Rutherford backscattering spectrometry (RBS) using 2 MeV ^{4}He ions and a scattering angle of 168°. Figure 1 shows RBS measurements of the Au distribution of sample *series I* prior to and after irradiation with 1×10^{16} cm^{-2} Sn ions. It is apparent, that the Au concentration profile remains essentially unchanged upon irradiation. Similar results have been observed for all irradiation doses for both sample series.

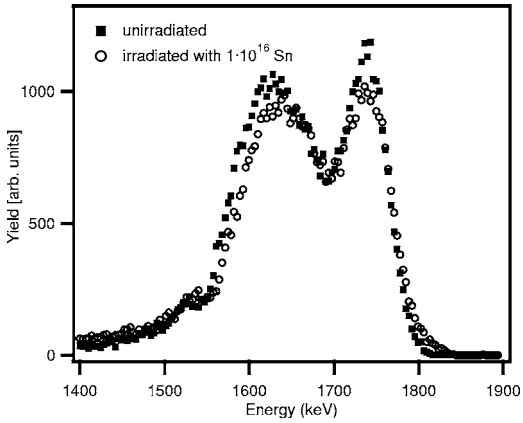

FIG. 1. RBS spectra of the Au implanted SiO_2 layer. The solid dots show the profile prior to irradiation and the open dots after irradiation with 1×10^{16} cm^{-2} Sn ions. For clarity only the Au peak is shown.

To provide a reference for our structural analysis, a 100 nm Au film was evaporated on SiO_2 and subsequently covered with 100 nm of SiO_2 deposited using plasma enhanced chemical vapor deposition (PECVD). These Au standards were irradiated simultaneously with the NPs. To study the possible influence of impurities on the atomic structure of ion irradiated Au we have implanted Si (60 keV, 7.5×10^{15} cm^{-2} and 200 keV, 5×10^{16} cm^{-2}) and O (30 keV, 5×10^{15} cm^{-2} and 110 keV, 5×10^{16} cm^{-2}) into a 100 nm Au film at liquid nitrogen temperature. Subsequently the Au film was irradiated with Sn under the same conditions as described above to an ion dose of 5×10^{15} cm^{-2}.

To prepare the NP samples for the EXAFS and SAXS measurements, the thin SiO_2 layer containing the NPs was isolated by removing the Si substrate via mechanical polishing and selective wet chemical etching in a KOH solution. To obtain an improved fluorescence signal in the EXAFS measurements, multiple layers of the thin implanted SiO_2 were mounted together on the sample holder between two layers of kapton. SAXS and EXAFS measurements were performed on the same samples.

Fluorescence EXAFS measurements at the Au *L*3 edge (11.919 keV) were performed at the Photon Factory, Japan (beamline 20-B) in an energy range between 11.70 and 13.48 keV, the latter corresponding to a photoelectron wave number (k) value of 20 $Å^{-1}$. Data were collected using a 10 element Ge solid-state detector. The Au *L*3 fluorescence signal comprised between 10% and 50% of the incoming count rate, with the latter maintained well within the linear region of the detector. Measurements were performed at a temperature of 10 K to reduce thermal vibrations. The AUTOBK code was used for background removal and normalization.[9] Extracted EXAFS spectra for sample *series I* are shown in Fig. 2. The spectra were analyzed using the FEFFIT program package.[10] EXAFS spectra were Fourier transformed (FT) over a k range of 4.7–16.2 $Å^{-1}$. Structural parameters were extracted from the first coordination shell which was isolated by inverse transforming over a non-phase-corrected radial distance range of 2.2–3.2 Å. The spectra were then fitted to the EXAFS equation including the first three moments of the

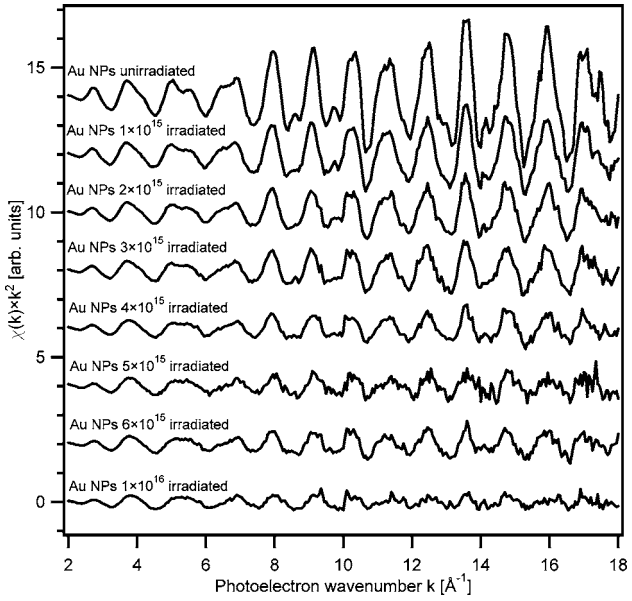

FIG. 2. k^2-weighted EXAFS spectra at 10 K of NP samples of *series I*. Irradiation doses are given in units of cm^{-2}.

interatomic distance distribution.[6] The amplitude reduction factor (S_0^2) and threshold energy (E_0) were determined from the unirradiated Au film and kept constant for fitting all spectra. The photoelectron scattering-path amplitudes and phases were calculated *ab initio* using FEFF8 (Ref. 11) for the face-centered-cubic (fcc) Au structure.

Transmission SAXS measurements were carried out at the ChemMatCARS beamline 15ID-D at the Advanced Photon Source, USA. We used 8.27 keV x rays (1.5 Å wavelength) at a camera length of 1870 mm. Scattering images were recorded with a Bruker 6000 CCD detector at an exposure time of 1 s on the same samples used for the EXAFS measurements to ensure comparability. Multiple images were recorded for each sample and averaged before analysis. An unimplanted SiO_2 film, prepared as described above, was measured to obtain the scattering contribution from the SiO_2 and kapton. For quantitative analysis we have used a maximum entropy method[12] (MEM) to determine the size distributions from the scattering spectra. Spherical shapes of the NPs were assumed as consistent with the TEM observations shown later.

III. RESULTS

Results of the SAXS measurements are shown in Fig. 3. Figure 3(a) shows the SAXS pattern of the unirradiated NPs of sample *series I* and the integrated spectra of the unirradiated NPs of both sample series. The scattering curve for the unirradiated NPs of sample *series I* shows a broad intensity maximum at low scattering vector q ($\sim$0.05 $Å^{-1}$). This indicates a dense NP population exhibiting a spatial correlation as has previously been observed for ion implanted Au NPs with a similar Au peak concentration.[13] In the spectrum for the unirradiated NPs of sample *series II*, however, no interference maximum can be observed although the Au concen-

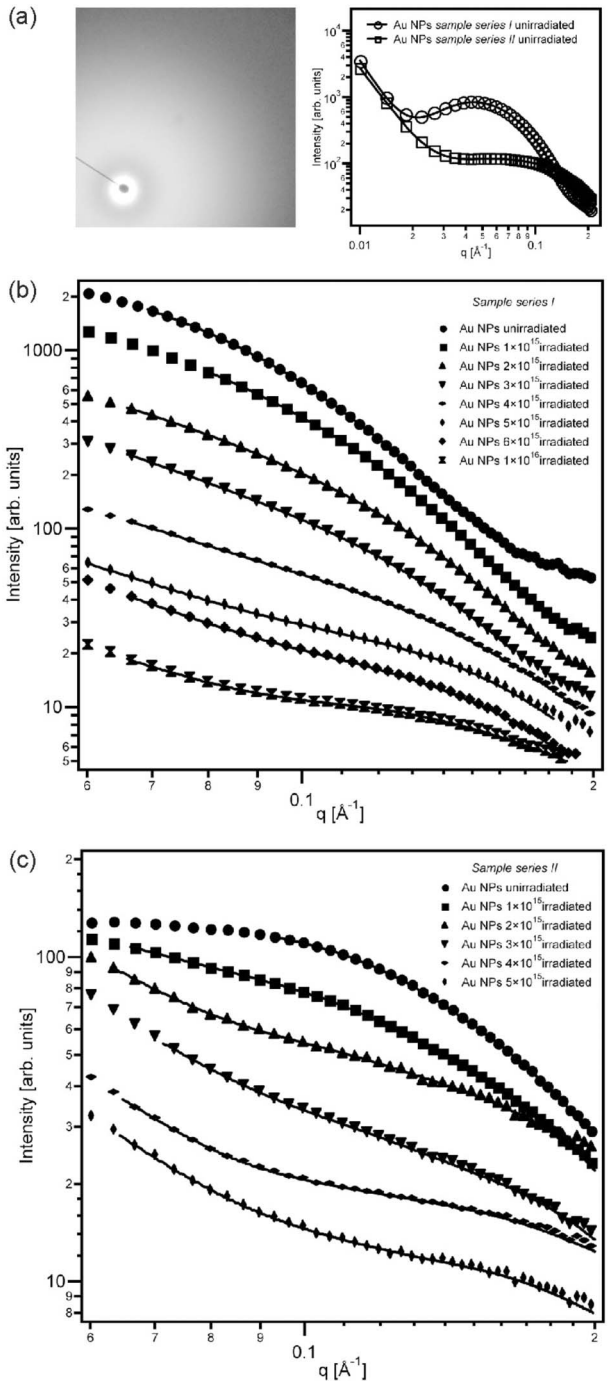

FIG. 3. (a) Recorded SAXS pattern of the unirradiated NPs of sample *series I* and the integrated spectra of the unirradiated NPs of both sample series. SAXS intensities for the NP samples of (b) sample *series I* and (c) sample *series II*. Irradiation doses are given in units of cm^{-2}. The solid lines show the corresponding fitted intensities using a maximum entropy method.

tration is the same as in sample *series I*. The different annealing conditions or equivalently the different NP growth conditions are a likely origin of this behavior as discussed below. Upon irradiation the maximum apparent in sample *series I* quickly vanishes and only spectra for the lowest two irradiation doses exhibit this feature (not shown). Figures 3(b) and 3(c) show SAXS spectra of sample *series I* and *II*, respectively, after background removal over a q-range of 0.06–0.2 Å^{-1}, covering the scattering contribution from the NPs. The solid lines show the corresponding fits which are in good agreement with the experimental data. Size distributions for both sample series as determined from the SAXS spectra are shown in Figs. 4(a) for sample *series I* and 4(b) for sample *series II*. Average NP diameters are given in Table I. Prior to irradiation we can observe a considerably wider size distribution with a larger average NP size for sample *series I* (O_2 anneals) as compared to *series II* (N_2/H_2 anneals). This is consistent with previous observations of Au NP formation and attributed to enhanced Au diffusion when annealed in oxidizing atmospheres.[8] Upon irradiation both NP distributions become narrower with a shift towards smaller NP sizes with increasing dose. In particular we can observe a significant decrease in the number of large NPs. This is consistent with simulations and previous experimental results on inverse Ostwald ripening and involves smaller particles growing at the expense of larger ones.[4] Cross-sectional TEM images in Fig. 5 confirm the largely spherical shape of the NPs prior to and following irradiation. This can be expected as at the given irradiation energies, nuclear stopping dominates and thus the memory of the incident beam direction is rapidly lost, resulting in rather isotropic collision cascades.[14] Figure 5(a) shows the unirradiated NPs of sample *series I*. The high resolution image indicates single crystalline particles and the electron diffraction pattern confirms the fcc structure present in bulk Au is retained in the NPs. Figure 5(b) shows the NPs after irradiation to a dose of 3×10^{15} cm^{-2}. We can clearly observe a population of small Au clusters between the larger NPs. After irradiation to a dose of 1×10^{16} cm^{-2} a nearly homogeneous size distribution is apparent with very few large NPs present as observable from the TEM image in Fig. 5(c). The TEM observations are in good agreement with the SAXS analysis.[4] We note that the given q range of the SAXS measurements and the much lower scattering intensity from smaller particles (compared to larger ones) somewhat limits the accuracy of the size distributions recovered by the MEM at the smaller diameters.[12] This should have only a small effect on the volume weighted average NP diameters which are dominated by the larger NPs. The existence of Au monomers and very small Au clusters (dimers, trimers…) however cannot be resolved using TEM or SAXS. We will later discuss that our EXAFS measurements indicate the formation of a large number of such monomers and small clusters.

Fourier-transformed, k^2-weighted EXAFS spectra are shown in Fig. 6 for (a) the unirradiated Au film and NP samples of both series and (b) for irradiated NPs of sample *series I*. The unirradiated NPs exhibit reduced peak amplitudes compared to the film spectrum. This reflects the decreasing average coordination number (CN) and the increasing Debye-Waller (D-W) factor, both a result of the significant SBR inherent with NPs. The atoms located at the NP surface are undercoordinated and as a consequence are expected to relax and/or reconstruct. The former yields the reduction in average CN and the latter leads to an increase in the D-W factor. The fcc structure, however, is retained as consistent with electron diffraction and previous investigations.[15,16] Upon irradiation a significant reduction of the

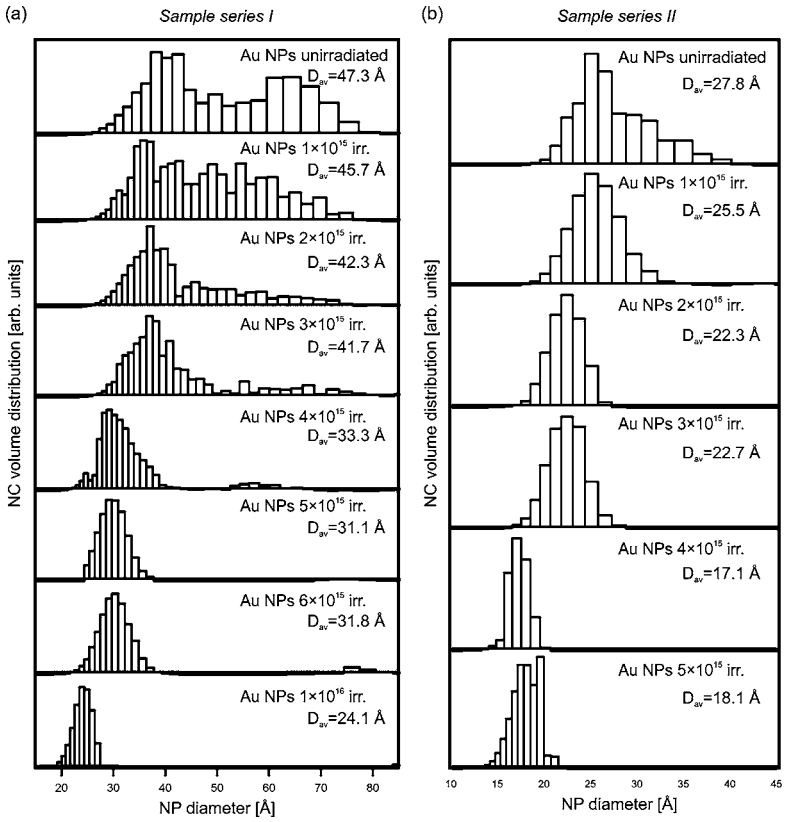

FIG. 4. Size distributions of the NP samples extracted from SAXS for (a) sample *series I* and (b) sample *series II*. Irradiation doses are given in units of cm^{-2}.

first nearest neighbor peak with a concomitant loss of higher order peaks (medium-range order) is apparent. The solid lines in Fig. 6 represent the corresponding first shell fits. Refined fitting parameters for all NP samples and the irradiated Au films are given in Table I. The reported errors are the fitting errors, i.e., the simulated spectra compared with the FT EXAFS spectra. *R* factors—a measure of the overall deviation of data and fits—are below 2.3% for all fits.

Figure 7 shows the (a) CN, (b) bond length (BL), and (c) D-W factor as a function of irradiation dose for both NP sample series as well as the Au films. It is apparent that all parameters remain virtually unchanged for the irradiated films while significant changes are evident for the NP samples. For both sample series, a large drop of the CN to a saturation value of approximately 4 can be observed as well as a general increase in the D-W factor, the latter trend is indicated by the dotted lines. For sample *series I* (the larger NPs) we can see a small BL expansion with respect to the unirradiated NPs for doses up to 3×10^{15} cm^{-2} followed by a BL contraction upon further irradiation. The smaller NPs show a decrease in BL for all irradiation doses.

IV. DISCUSSION

In the following we will discuss the effects of ion irradiation on the NP structural parameters measured by EXAFS, in particular the BL and CN. To separate such effects from changes that are only related to the reduction in NP size, we have plotted the BL and CN versus average NP size measured by SAXS in Fig. 8 (values are listed in Table I), along with theoretical, size dependent expectations. The deviation from these expectations (and the good agreement with unirradiated NPs) demonstrates the effects induced by ion irradiation.

NPs typically exhibit a size dependent BL contraction relative to bulk material (for example see Refs. 17 and 18). For Au NPs this can be described surprisingly well in terms of surface tension due to the high SBR using a simple liquid drop (LD) model given by $\Delta R=-\frac{4}{3}KR_b f\frac{1}{D}$,[19] where K is the bulk compressibility, and R_b the bulk metal BL, and f the surface tension. We have previously obtained a value of 3.4 ± 0.5 J/m^2 for the surface tension of Au NPs formed by ion implantation.[13] This value is in good agreement with those extracted from TEM measurements of Au NPs formed by ion beam synthesis (4 J/m^2) (Ref. 20) and EXAFS measurements of evaporated Au NPs (3.46 ± 0.42 J/m^2) (Ref. 21). Although this macroscopic model can only be considered a crude approximation, in particular for small clusters, the interatomic distance in Au dimers deviates only marginally from the model. The reported BL contraction $R_{dimer}/R_{nn}=0.86$,[22] where R_{dimer} and R_{nn} are the BLs of the dimer and bulk, respectively, is slightly larger than the 0.93 ± 0.2 predicted by the LD model. The BL contraction as extracted from EXAFS is shown as a function of the average NP diameter measured by SAXS for both sample series in Fig. 8(a). The solid line shows the LD model with the dashed lines displaying the error associated with the experimental value for the surface tension. Both unirradiated NP samples are in excellent agreement with the LD model. We note that for a given sample series, the average NP size decreases as the irradiation dose increases as first presented in Fig. 4. Given this decrease and the expected BL contraction due to surface tension, the deviation of the BL measured for our NP

TABLE I. Refined fitting parameters from EXAFS analysis of the first coordination shell as a function of ion irradiation dose (in units of cm^{-2}). N, R, σ^2, and C_3 are the coordination number, bond length, Debye-Waller factor, and third order cumulant, respectively. Also listed are the average NP diameters as extracted from the SAXS measurements. The corresponding CNs are given as evaluated by Eq. (1).

	EXAFS				SAXS	
	CN	*R* (Å)	σ^2 (10^{-3} Å^2)	C_3 (10^{-4} Å^3)	D_{av} (Å)	CN_{cal}
Au films						
Au film unirradiated	12 (fixed)	2.862±0.016	1.4±0.2	−0.4±0.8[a]	N/A	N/A
Au film 1×10^{15} irr.	13.0±0.7	2.867±0.003	1.7±0.2	−0.1±0.2	N/A	N/A
Au film 3×10^{15} irr.	12.6±1.0	2.861±0.004	1.8±0.2	−0.5±0.4	N/A	N/A
Au film 6×10^{15} irr.	12.2±1.0	2.867±0.004	1.6±0.2	−0.1±0.3	N/A	N/A
Au film 1×10^{16} irr.	12.1±0.7	2.865±0.003	1.6±0.2	−0.2±0.3	N/A	N/A
NP series I						
NPs unirradiated	11.5±0.8	2.845±0.004	2.3±0.2	−0.6±0.3	47.3	10.9
NPs 1×10^{15} irr.	8.5±0.6	2.857±0.004	2.8±0.2	0.1±0.3	45.7	10.9
NPs 2×10^{15} irr.	6.5±0.3	2.851±0.002	2.9±0.1	−0.2±0.2	42.3	10.8
NPs 3×10^{15} irr.	5.8±0.4	2.848±0.004	3.0±0.2	−0.5±0.3	41.7	10.8
NPs 4×10^{15} irr.	4.0±0.3	2.841±0.003	3.0±0.2	−0.6±0.3	33.3	10.5
NPs 5×10^{15} irr.	3.8±0.3	2.815±0.005	4.0±0.3	−1.8±0.4	31.1	10.4
NPs 6×10^{15} irr.	4.3±0.3	2.829±0.004	3.7±0.2	−1.8±0.3	31.8	10.4
NPs 1×10^{16} irr.	3.8±0.5	2.800±0.008	6.0±0.6	−3.3±0.8	24.1	9.9
NP series II						
NPs unirradiated	9.7±1.1	2.832±0.007	4.9±0.4	−1.0±0.6	27.8	10.2
NPs 1×10^{15} irr.	6.1±0.7	2.830±0.006	4.7±0.4	−0.2±0.6	25.5	10.0
NPs 2×10^{15} irr.	4.8±0.3	2.812±0.004	6.0±0.3	−0.6±0.4	22.3	9.7
NPs 3×10^{15} irr.	4.1±0.9	2.828±0.012	3.7±0.8	−1.5±1.0	22.7	9.8
NPs 4×10^{15} irr.	4.1±0.5	2.787±0.008	8.0±0.7	−2.5±1.0	17.1	9.1
NPs 5×10^{15} irr.	3.9±0.8	2.772±0.011	7.9±1.0	−2.5±1.5	18.1	9.2

[a]C_3 was included in the fit for the Au film to provide a reference for the following fits of the NP samples and can be interpreted as a small offset.

systems from the LD model yields information about irradiation induced effects. For sample *series I* we observe an expansion of the BL with respect to the model for the lower irradiation doses, then a significant contraction for the higher doses. For sample *series II*, the initially smaller NPs, a contraction is apparent only at the higher irradiation doses. At lower irradiation doses the BL agrees with the model.

As discussed above, a reduction in the NP size leads to a decrease in the average CN due to the increased SBR or equivalently the relative increase in undercoordinated surface atoms. Figure 8(b) shows the CNs for both sample series as a function of the average NP diameter measured by SAXS. The dotted line in Fig. 8(b) shows the size dependent average CN of a 12-fold coordinated spherical Au NP. This can be estimated by

$$CN_{NP} = 12\left(1 - \frac{3}{2D}R_{nn}\right) \quad (1)$$

(Ref. 23), where R_{nn} is the BL and D is the average NP diameter. After ion irradiation, we can see a dramatic difference in the average CN obtained by EXAFS compared to that calculated with (1) with the diameter measured by SAXS. Prior to ion irradiation, the CNs are in good agreement for both techniques. For both sample series, we will argue below, that the deviation of BLs and CNs from the model assumptions at high irradiation doses is the result of monomer and/or small cluster formation.

We now discuss potential causes of the observed behavior of the structural parameters of the irradiated NPs.

Irradiation induced disorder in the NPs. For lower irradiation doses, the observed BL expansion (observed in sample *series I*) and CN reduction is consistent with a disordered NP phase. Generally, an increase in disorder is reflected in an increase in D-W factor which we can observe with increasing irradiation dose. An increase can also result from the decrease in NP size and the associated increase in the SBR. The undercoordinated Au atoms at the surface are relaxed/reconstructed and lead to a broadening of the interatomic distance distribution. For unirradiated NPs we would expect the BL distribution to be asymmetric and skewed to a shorter BL as relaxed/reconstructed metal surfaces generally contract. An asymmetric deviation from a Gaussian bond length distribution is manifested as a nonzero third moment or cumulant C_3. Previous EXAFS measurements on ion implanted Au NPs show the expected negative C_3 (distribution skewed to shorter BL).[15] At lower irradiation doses the

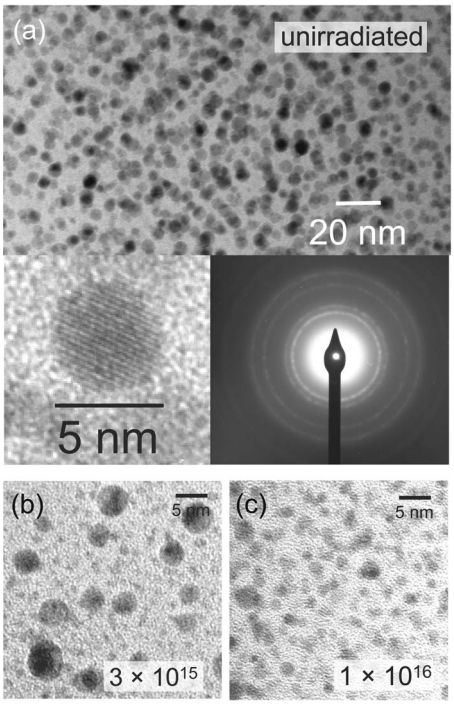

FIG. 5. Cross-sectional TEM images of Au NPs of sample *series I* (a) unirradiated, (b) after irradiation with 3×10^{15} cm^{-2} Sn ions, and (c) after irradiation with 1×10^{16} cm^{-2} Sn ions. The insets in (a) show a high-resolution image and the corresponding electron diffraction pattern.

present experiments show an increase in C_3. A BL expansion and a BL distribution skewed to longer BLs are consistent with theoretical predictions from a dense random packing model for amorphous metals[24] and agree well with recent investigations of ion irradiated[25] Cu NPs and structural investigations on sonochemically prepared amorphous iron.[26] These studies also report a decrease in the CN in the disordered phase. Although bulk elemental metals cannot be rendered amorphous using ion implantation (with one reported exception[27] for Ga), NPs have shown a significantly increased susceptibility to irradiation damage compared to bulk material.[28] The ion-irradiation induced crystalline-to-amorphous phase transition in Si and Ge NPs was shown to occur at irradiation doses significantly lower than those required for bulk material.[28–30] This was attributed to the higher structural energy state of the NPs and possible preferential nucleation of the amorphous phase at the NP/matrix interface. An increased D-W factor and a BL expansion have also been observed for irradiation of Ag NPs using low-mass ions.[31] We will later discuss the influence of the generation of monomers and small clusters on the measured structural parameters of Au NPs.

Impurity effects in the NPs. The incorporation of impurities into pure metals can stabilize an amorphous phase.[32] To assess the possible influence of recoiling Si and O atoms on the NP structure, we implanted Si and O into a thin Au film to a total concentration of approximately 10 at. %. Subsequently this film was irradiated with 5×10^{15} cm^{-2} Sn ions under the same conditions as the NPs. EXAFS measurements are summarized in Table II. A slight increase in the D-W

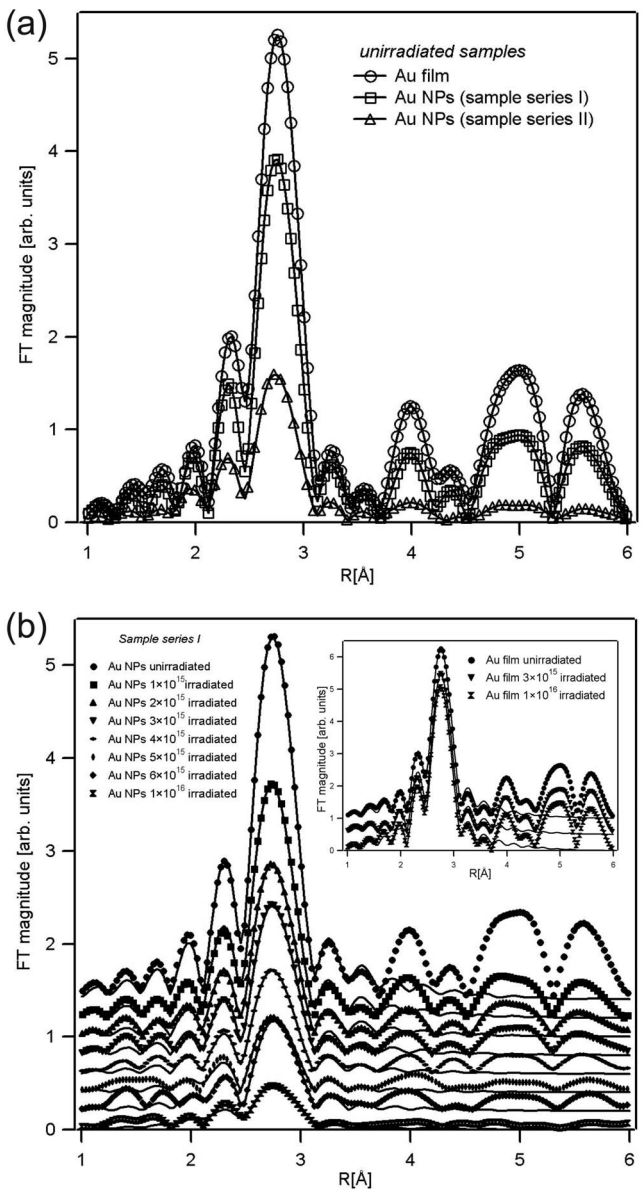

FIG. 6. Fourier-transformed, k^2-weighted EXAFS spectra for (a) the unirradiated Au film and NP samples of both series and (b) for all NP samples of *series I*. The solid lines in (b) show the corresponding fits of the first coordination shell. The inset shows selected spectra of unirradiated and irradiated Au films for comparison.

factor can be observed. The BL and CN, however, remain virtually unchanged. Thus, we believe, that impurities are not responsible for the observed structural changes in the NPs at low irradiation doses.

Generation of monomers and small Au clusters due to collisional mixing. During the irradiation process, collision cascades lead to the observed evolution of the size distribution due to inverse Ostwald ripening. Au atoms are detached from larger NPs and then attach to smaller clusters or form nucleation sites for new clusters. As apparent from the TEM images in Fig. 5, we observe the evolution of a population of small Au NPs between the larger ones. Precursors in the form of Au monomers and small Au clusters (dimers, trimers,…) will also be present in the SiO_2. These atoms/clusters

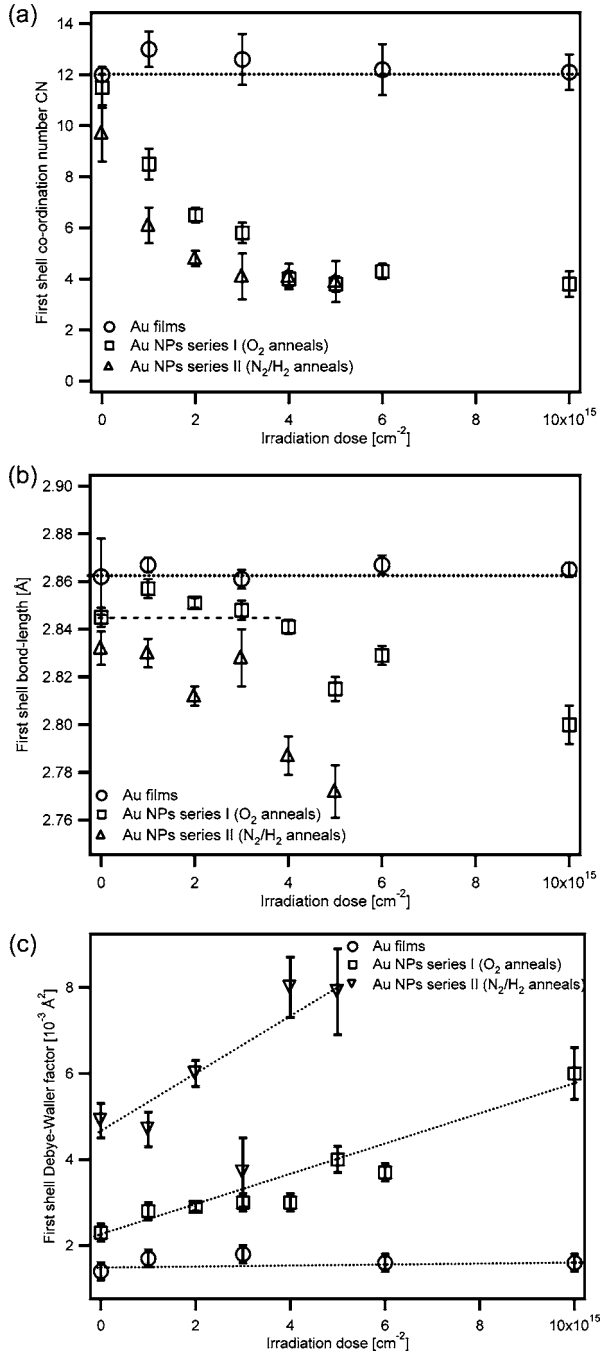

FIG. 7. Refined EXAFS parameters (a) CN, (b) Au-Au bond length, (c) D-W factor extracted from the first coordination shell for Au NP samples and Au films as function of ion irradiation dose given in units of cm^{-2}. The dotted lines are plotted to indicate general trends. The dashed line in (b) shows the value for the unirradiated NPs of sample *series I* to highlight the bond length increase at low irradiation doses.

are too small to be detected by TEM and SAXS. EXAFS, however, measures the average atomic environment around *all* Au atoms. Au monomers dissolved in the SiO_2 matrix will only affect the refined CN as they contribute to the absorption but not to the EXAFS oscillation originating from Au-Au bonding. The normalization of the EXAFS signal to the absorption will then cause an effective reduction in the

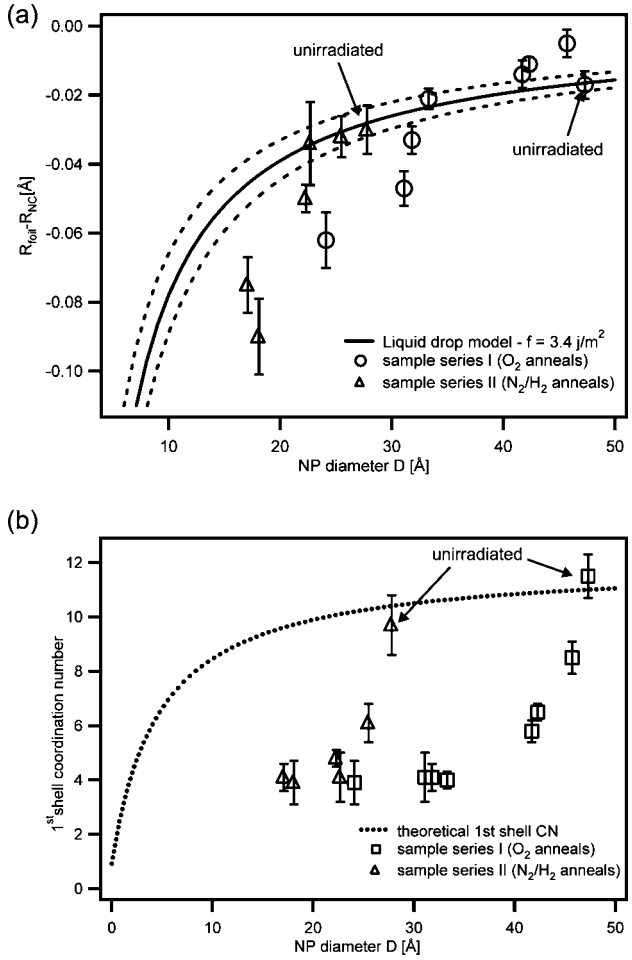

FIG. 8. (a) Au-Au bond length and (b) CN as a function of NP diameter as extracted from SAXS. The solid line in (a) shows the bond length contraction expected from a simple liquid-drop model using a surface tension value of 3.4 ± 0.5 J/m^2 (Ref. 14) (the dashed lines represent the associated error). The dotted line in (b) shows the expected CN for a spherical (fcc) NP. For a given sample series, the NP size decreases as the irradiation dose increases.

EXAFS amplitude which appears as a reduction of the CN with respect to the bulk material. No additional peaks can be observed in the Fourier transformed EXAFS spectra in Fig. 6(b) given the probable disordered environment about a Au monomer and the weak scattering from the matrix constituents relative to Au. Small clusters with very low Au coordinations (1 for dimers, 2 for trimers, …) also yield a decrease in the measured average CN. The presence of both monomers and small clusters can explain the large decrease in the CN measured by EXAFS and the large difference compared to the prediction. Small clusters additionally affect the simulated parameters for the first Au-Au coordination shell such as BL, D-W factor, and C_3. The greater than expected reduction in BL (for the higher irradiation doses) with the large deviation from the LD model is consistent with the formation of small Au clusters that cannot be detected by SAXS or TEM. This is also consistent with the increasing negative values for C_3 at the higher irradiation doses. A large number of small clusters with the highly contracted BLs results in a BL distribution effectively skewed to small values.

TABLE II. Refined fitting parameters from EXAFS analysis of the first coordination shell of Au films. N, R, σ^2, and C_3 are the coordination number, bond length, Debye-Waller factor, and third order cumulant, respectively.

	CN	R (Å)	σ^2 (10^{-3} Å^2)	C_3 (10^{-4} Å^3)
Au film	12 (fixed)	2.868±0.010	1.9±0.2	−0.1±0.5
Au film+O+Si	11.1±0.5	2.864±0.002	2.2±0.1	−0.3±0.2
Au film+O+Si 5×10^{15} irr.	11.8±0.7	2.867±0.003	2.2±0.2	−0.2±0.3

The observed narrowing of the size distribution as well as the nucleation of new NPs under ion irradiation has been predicted by kinetic Monte Carlo simulations, where the irradiation temperature is far below a critical temperature[3] T_c (T_c is defined as the temperature above which the NP size distribution widens due to conventional Ostwald ripening and below which narrows by inverse Ostwald ripening). The observed formation of a significant fraction of monomers and small clusters in our experiments agrees well with the authors' predicted high solute concentration and the early stages of nucleation for temperatures far below T_c.

Using the difference between the CN predicted by equation (1) CN_{NP} (using NP sizes extracted from SAXS) and the CN measured by EXAFS (CN_{EX}) we can estimate the volume fraction of Au present as monomers and small clusters as $V_{rel}=\frac{V_{cl}}{V_{tot}}=\frac{CN_{NP}-CN_{EX}}{CN_{NP}-CN_{cl}}$, where V_{cl} is the volume of Au in monomers and small clusters, V_{tot} is the total volume of Au atoms and CN_{cl} the average Au coordination number of the small clusters (0 for monomers, 1 for dimers,…). Figure 9 shows the volume fraction of Au in monomers and small clusters as a function of irradiation dose (for sample *series I*) and CN_{cl}. For example, at an irradiation dose of 1×10^{15} cm^{-2}, if only monomers are present ($CN_{cl}=0$), approximately 20% of all Au atoms are dispersed in the matrix. If the dispersed Au was present as only dimers ($CN_{cl}=1$) this fraction would increase to approximately 25%. Naturally we expect a mixture of cluster sizes together with a fraction of monomers. As apparent from Fig. 9, the fraction of dispersed Au increases with increasing irradiation dose as expected due to the ongoing intermixing. For irradiation doses greater than 4×10^{15} cm^{-2}, where CN_{EX} saturates at ~4, the graph no longer changes significantly (not shown). However, the continuing BL contraction indicates a further increase in cluster formation and thus an ongoing increase in V_{rel}.[33]

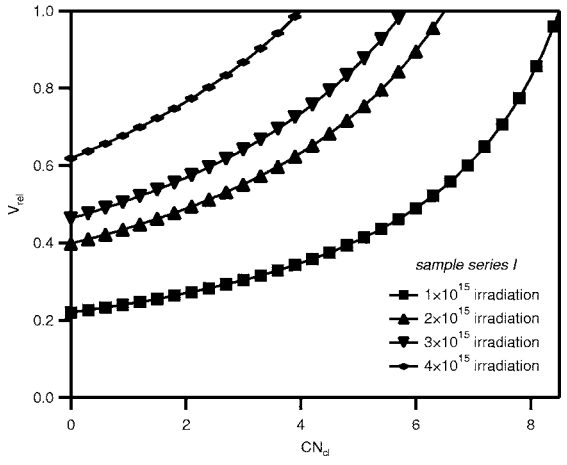

FIG. 9. Estimated volume fraction of Au dispersed in the SiO_2 (as monomers and small clusters) as a function of the average CN of small clusters (monomers=0) shown for selected irradiation conditions for sample *series I*.

Quantification of the effects discussed above on the measured structural parameters is difficult. Our measurements suggest that with increasing irradiation dose, the generation of monomers/small clusters due to mixing dominate the parameters extracted by EXAFS. For the initially smaller NPs (sample *series II*) the mixing effects—as indicated by the large drop in BL and CN—set in at lower irradiation doses as expected. This is also apparent from the steeper increase in the D-W factor for sample *series II* [see Fig. 7(c)]. The large number of Au monomers and small clusters forming during ion irradiation is somewhat surprising as in previous studies we observed the formation of Au NPs immediately upon implantation of low concentrations (~0.4 at. %) at liquid nitrogen temperature.[16] The experimental CN (~8) was in good agreement with that predicted from the measured NP size, implying a negligible fraction of Au monomers. This suggests a high mobility of Au atoms at these low temperatures possibly stimulated by irradiation enhanced diffusion. Differences in the cascade size and density may account for the observed differences in monomer fraction. Furthermore, as consistent with the high cohesive energy of the Au atoms, we have no evidence for the formation of mixed (Au/Si/O) NPs.

V. CONCLUSIONS

In conclusion, we have studied the effect of ion irradiation on the size and structural evolution of ion beam synthesized Au NPs using a combination of EXAFS and SAXS. We observed a narrowing of the NP size distribution consistent with inverse Ostwald ripening while the NPs largely retain their spherical shape. At lower irradiation doses an effective BL expansion and a distribution skewed to longer BLs provide evidence for the formation of a disordered NP phase consistent with amorphous material. A significant drop of the CN and a large BL contraction at higher irradiation doses indicate the generation of Au dispersed as monomers and small clusters in the SiO_2 due to collisional mixing. Our results present potential applications in tuning the optical properties of the embedded NPs, including the surface plasmon resonance, and as such they are interesting for utilization in advanced microoptical device fabrication.

ACKNOWLEDGMENTS

P.K. and M.C.R. thank the Australian Research Council for support. P.K., B.J., D.J.C., G.J.F., and M.C.R. were supported by the Australian Synchrotron Research Program, which is funded by the Commonwealth of Australia under the Major National Research Facilities Program. P. Kluth is grateful to the Humboldt Foundation in Germany for support. ChemMatCARS Sector 15 at the Advanced Photon Source is principally supported by the National Science Foundation/Department of Energy under Grant No. CHE0087817 and by the Illinois Board of Higher Education. The Advanced Photon Source is supported by the U.S. Department of Energy, Basic Energy Sciences, Office of Science, under Contract No. W-31-109-Eng-38.

*Corresponding author. Electronic mail: patrick.kluth@anu.edu.au

[1] U. Kreibig, H. Boennemann, J. Hormes, in *Handbook of Surfaces and Interfaces of Materials*, edited by H. S. Nalwa (Academic, San Diego, 2001), Vol. 3, pp. 2–85.
[2] K. Trachenko, J. M. Pruneda, E. Artacho, and M. T. Dove, Phys. Rev. B **71**, 184104 (2005).
[3] K. H. Heinig, T. Mueller, B. Schmidt, M. Strobel, and W. Moeller, Appl. Phys. A **77**, 17 (2003).
[4] P. Kluth and M. C. Ridgway, Nucl. Instrum. Methods Phys. Res. B **242**, 458 (2006).
[5] C. D'Orleans, J. P. Stoquert, C. Estournes, C. Cerruti, J. J. Grob, J. L. Guille, F. Haas, D. Muller, and M. Richard-Plouet, Phys. Rev. B **67**, 220101(R) (2003).
[6] E. A. Stern, Phys. Rev. B **10**, 3027 (1974).
[7] A. I. Frenkel, C. W. Hills, and R. G. Nuzzo, J. Phys. Chem. B **105**, 12689 (2001), and references therein.
[8] A. Miotello, G. De Marchi, G. Mattei, P. Mazzoldi, and C. Sada, Phys. Rev. B **63**, 075409 (2001).
[9] M. Newville, P. Livins, Y. Yacoby, J. J. Rehr, and E. A. Stern, Phys. Rev. B **47**, 14126 (1993).
[10] M. Newville, B. Ravel, D. Haskel, J. J. Rehr, E. A. Stern, and Y. Yacoby, Physica B **208-209**, 154 (1995).
[11] A. L. Ankudinov, B. Ravel, J. J. Rehr, and S. D. Conradson, Phys. Rev. B **58**, 7565 (1998).
[12] C. S. Tsao and T. L. Lin, J. Appl. Crystallogr. **30**, 353 (1997).
[13] P. Kluth, B. Johannessen, D. J. Cookson, G. J. Foran, and M. C. Ridgway, Nucl. Instrum. Methods Phys. Res. B **246**, 30 (2006).
[14] S. Klaumünzer, Nucl. Instrum. Methods Phys. Res. B **244**, 1 (2006).
[15] P. Kluth, B. Johannessen, V. Giraud, A. Cheung, C. J. Glover, G. de M. Azevedo, and M. C. Ridgway, Appl. Phys. Lett. **85**, 3561 (2004).
[16] P. Kluth, B. Johannessen, C. J. Glover, G. J. Foran, and M. C. Ridgway, Nucl. Instrum. Methods Phys. Res. B **238**, 285 (2005).
[17] B. Gilbert, F. Huang, H. Zhang, G. A. Waychunas, and J. Banfield, Science **305**, 651 (2004).
[18] B. Johannessen, P. Kluth, C. J. Glover, G. de M. Azevedo, D. J. Llewellyn, G. J. Foran, and M. C. Ridgway, J. Appl. Phys. **98**, 024307 (2005).
[19] C. W. Mays, J. S. Vermaak, and D. Kuhlmann-Wilsdorf, Surf. Sci. **12**, 134 (1968).
[20] G. De Marchi, G. Mattei, P. Mazzoldi, C. Sada, and A. Miotello, J. Appl. Phys. **92**, 4249 (2002).
[21] A. Balerna, E. Bernieri, P. Picozzi, A. Reale, S. Santucci, E. Burattini, and S. Mobilio, Surf. Sci. **156**, 206 (1985).
[22] P. J. Feibelman, Phys. Rev. B **53**, 13740 (1996).
[23] S. de Panfis, F. d'Aacapito, V. Haas, H. Conrad, J. Weissmueller, and F. Boscherini, Phys. Lett. A **207**, 397 (1995).
[24] L. v Heimendahl, J. Phys. F: Met. Phys. **5**, L141 (1975).
[25] B. Johannessen, P. Kluth, D. J. Llewellyn, G. J. Foran, D. J. Cookson, and M. C. Ridgway (unpublished).
[26] G. J. Long, D. Hautot, Q. A. Pankhurst, D. Vandormael, F. Grandjean, J. P. Gaspard, V. Briois, T. Hyeon, and K. S. Suslick, Phys. Rev. B **57**, 10716 (1998).
[27] M. Holz, P. Ziemann, and W. Buckel, Phys. Rev. Lett. **51**, 1584 (1983).
[28] M. C. Ridgway, G. de M. Azevedo, R. G. Elliman, C. J. Glover, D. J. Llewellyn, R. Miller, W. Wesch, G. J. Foran, J. Hansen, and A. Nylandsted-Larsen, Phys. Rev. B **71**, 094107 (2005).
[29] D. Pacifici, E. C. Moreira, G. Franzo, V. Martorino, F. Priolo, and F. Iacona, Phys. Rev. B **65**, 144109 (2002).
[30] D. Pacifici, G. Franzo, F. Iacona, and F. Priolo, Physica E (Amsterdam) **16**, 404 (2003).
[31] F. d'Acapito, F. Gonella, E. Cattaruzza, S. Pascarelli, P. Mazoldi, and S. Mobilio, Nucl. Instrum. Methods Phys. Res. B **120**, 110 (1996).
[32] C. Cohen, A. Benyagoub, H. Bernas, J. Chaumont, L. Thome, M. Berti, and A. V. Drigo, Phys. Rev. B **31**, 5 (1985).
[33] These considerations are based on the assumption that the CN in the NPs is not altered due to structural changes induced by the irradiation.